

Table 2. Effect of thymic lymphoma involvement on concentration of ^{67}Ga in AKR/J mouse thymus.

Degree of involvement (%)	Animals (No.)	Thymic concentration	
		(% dose/g)	(S.E.)
5 or less	8	2.5	± 0.4
50 or more	10	16.5	± 2.0

(2). The transplantable neoplasm of rats (RFT) showed the greatest affinity for ^{67}Ga on both an absolute and relative basis. This slow-growing tumor (5) is readily transplanted and through eight serial passages has maintained the same growth rate and characteristic histologic pattern. In two rats studied 4 months after intramuscular transplantation, when the tumors were large and beginning to ulcerate, small pulmonary, adrenal, and lymph-node metastases have been demonstrated.

A comparison of the deposition of ^{67}Ga in viable and necrotic tumor indicated that the uptake of gallium is primarily associated with viable tumor tissue. In the two rats with metastasizing RFT tumors the average ratio of the ^{67}Ga concentration in viable tumor to that in necrotic tumor was 33. This pattern of distribution was confirmed with autoradiography. In the R-3259 giant cell sarcoma the average ratio was 11 and in the Walker-256 carcinosarcoma it was 4. Gross visual distinction between viable and necrotic tumor could not readily be made in the other tumors studied.

The AKR/J mouse becomes "spontaneously leukemic" at an age of 6 to 12 months, with the onset preceded by thymic atrophy and followed by atypical hyperplasia (7). Frank neoplasm is first manifested by a focal lymphomatous involvement of the thymus. This early lymphomatous stage provided a model for studying the deposition of gallium in a malignant neoplasm infiltrating the organ of origin. Eight- to ten-month-old AKR/J mice were given ^{67}Ga and killed 1 day later. Each thymus was assayed for ^{67}Ga content and studied histologically for estimation of the percentage of involvement with lymphoma. For comparison the mice were divided into two groups: (i) those with lymphoma comprising 5 percent or less of the histologic sections of thymus, and (ii) those with lymphoma occupying 50 percent or more. The results of this study are shown in Table 2. Gal-

lium-67 concentration in the group with massive lymphomatous involvement was 6.6 times that of the group with minimal involvement; the difference between the two groups was highly significant.

The nature of the affinity of viable rat and mouse tumor tissue for gallium is not clear. However, light and electron microscopic autoradiography of RFT and ESR-586 tumor tissues indicate that ^{67}Ga is concentrated in the cytoplasm of neoplastic cells. Figure 1 shows a microscopic autoradiogram of a section of RFT tumor ($\sim 0.5 \mu\text{m}$ thick) together with an electron microscopic autoradiogram of the same tumor. Further evidence that the deposition of gallium is intracellular is provided by the fact that 80 percent of the ^{67}Ga activity in homogenates of the RFT tumor could be spun down in an ultracentrifuge; only 20 percent of the activity remaining in the supernatant was dialyzable.

Gallium-67 has been tested for localization in seven nonosseous rat and mouse tumors. Deposition in tumor tissue was variable but distinct; a new rat tumor developed in our laboratory showed the most specific uptake and has been adopted as a model for further studies. A high concentration of ^{67}Ga was observed in the AKR/J mouse thymus in the presence of massive thymic involvement with lymphoma. Gallium concentrates mainly in viable rather than in necrotic tumor cells and is most likely bound to an intracellular cytoplasmic component.

These results suggest that ^{67}Ga , with its remarkable ability to concentrate in living malignant cells, may be useful not only in clinical diagnostic applications, but also in studies of the nature of malignant change.

R. L. HAYES, B. NELSON

D. C. SWARTZENDRUBER

J. E. CARLTON, B. L. BYRD

Medical Division, Oak Ridge

Associated Universities,

Oak Ridge, Tennessee 37830

References and Notes

1. C. L. Edwards and R. L. Hayes, *J. Nucl. Med.* **10**, 103 (1969).
2. H. C. Dudley, *J. Pharmacol. Exp. Ther.* **95**, 482 (1949); M. Brucer, *Radiology* **61**, 534 (1953); R. L. Hayes, in *Radioactive Pharmaceuticals*, G. A. Andrews, R. M. Kniseley, H. N. Wagner, Jr., Eds. (AEC Symposium Series No. 6, CONF-651111, April 1966), p. 603.
3. Obtained from the Isotopes Development Center, Oak Ridge National Laboratory, Oak Ridge, Tennessee.
4. Millipore filters from the Millipore Corporation, Bedford, Massachusetts.
5. The experimental rat tumors used in this study were (i) R-3259 giant cell sarcoma, originally from Dr. W. F. Dunning, University

of Miami, Coral Gables, Florida; (ii) Walker-256 carcinosarcoma, originally from Dr. Enrico Mihich, Roswell Park Memorial Institute, Buffalo, New York; and (iii) RFT, a poorly differentiated rat malignancy, obtained from Dr. Frank Comas of this laboratory. This tumor arose from the skin or subcutaneous tissues of the thigh of a Fischer-344 rat surviving total-body gamma irradiation. The four mouse tumors used were (i) ESR-586 preputial gland tumor, originally purchased from The Jackson Laboratory, Bar Harbor, Maine, and supplied to us by Dr. Fred Snyder of this laboratory; (ii) P-1798 lymphosarcoma provided by Mr. Isidore Wodinsky of Arthur D. Little, Inc., Cambridge, Massachusetts; (iii) C3H/HeJ strain spontaneous mammary tumor; and (iv) AKR/J strain leukemia. The last two types of mice were purchased from The Jackson Laboratory.

6. For purposes of comparison, the individual tumor concentration values (percent administered dose per gram) have been normalized to an average body weight of 25 g for mice and 250 g for rats. Accordingly, the mouse tumor concentrations should be divided by 10 for comparison with those of the rat.
7. K. Arnesen, *Acta Pathol. Microbiol. Scand.* **43**, 350 (1958).
8. Under contract with U.S. Atomic Energy Commission.

13 October 1969

Conformations at Local Energy Minima for Gramicidin S: Optical Calculations

Abstract. Energy minimization techniques applied to an arbitrary peptide primary sequence result in a still large number of hypothetical structures of similar energy. Optical activity calculations can, in principle, be used to screen the low-energy conformations. Those conformations which yield a spectrum different from the observed spectrum by a factor greater than the current reliability of the calculation can be excluded. The method is applied to gramicidin S.

The two empirical uses of measurements of biopolymer optical activity have been the detection of regions of regular conformations in proteins and nucleic acids and the detection of changes in their conformations upon environmental perturbation. It is worthwhile to seek additional applications of any increased understanding of optical properties of biopolymers.

I propose that theoretical calculations of optical properties of polypeptides may soon be reliable enough to screen the low-energy conformations generated by minimization routines from primary sequences, allowing those conformations, whose calculated spectrum differs from the experimental spectrum by a factor greater than the current reliability of the calculations, to be discarded. As the dependability of the optical calculations improves, more of the low-energy conformations

could be excluded until, in principle, that conformation giving the calculated spectrum closest to the experimental one could be selected as best describing the true conformation.

At the present time, the confidence limits of the spectral calculations are such that few local minimum conformations would be excluded in the case of an arbitrary peptide; which is not to say, of course, that the conformations are undistinguishable by experimental optical measurements. Furthermore, the entire procedure is only applicable to peptides which have a well-defined equilibrium conformation. In spite of these limitations, being able to combine the fields of conformational energy calculations, experimental optical measurements, and spectral calculations is appealing enough to warrant the demonstration here of the suggested procedure in the case of a peptide severely restricted in configurational space—the monocyclic decapeptide antibiotic, gramicidin S.

Craig suggests a unique configuration for this molecule at equilibrium in solution (1), and several models have been proposed separately, based on either x-ray data on the solid (2); chemical (3), optical (4), proton exchange (5), or magnetic resonance (6, 7) data on solutions; or theoretical energy minimization procedures (8). These models have been specified to varying degree of detail, but it is nevertheless clear that there are large differences in the proposed structures.

Scott *et al.* (9) and Momany *et al.* (10) have reported the potential energy surface of the molecule generated by their approximation to the potential energy function. They have located a number of the local minimums in the energy surface and found structures similar to several of the models. Three of these structures were used here to define the set of conformations to be screened.

The calculation of rotational strengths by configuration interaction of excited states has been described (11). A column vector \mathbf{u} is defined with αN elements, each element being a three-dimensional column vector. The α_i th N elements contain the electric transition moments of the α_i th transition for the N noninteracting monomers. An analogous matrix \mathbf{m} can be defined for the αN noninteracting magnetic moments. If \mathbf{H} is the αN -dimensional interaction matrix, and \mathbf{T} is the unitary matrix which diagonalizes it, the column vectors $\mathbf{T}\mathbf{u}$ and $\mathbf{T}\mathbf{m}$, where each

Table 1. Calculated b_0 parameters for three proposed gramicidin S solution structures which have also been located at minimums of the approximate potential energy surface of the molecule. Model I has the structure GS_{V} (10). Structure GS_{VI} (10) is similar and yields a b_0 of -364° . Model II has the structure GS_{III} (9). Model III has the structure GS_{Ia} (9). For the experimentally measured value of b_0 for gramicidin S see (16).

Structure	b_0 (deg)
Model I	-254
Model II	+ 17
Model III	+ 23
Gramicidin S (experiment)	-720 ± 90

\mathbf{T} element multiplies all three spatial components of each \mathbf{u} and \mathbf{m} element, give, respectively, the electric and magnetic moments of the interacting monomers. The absorption and rotational strengths are therefore given by column vectors \mathbf{A} and \mathbf{R} , the k th elements of which are $(\mathbf{A})_k = (T\mu)_k(T\mu)_k$ and $(\mathbf{R})_k = \text{Im}(T\mu)_k(Tm)_k$.

The diagonal elements of \mathbf{H} are taken to be the transition energies experimentally observed in the spectrum of a suitable model compound, and the off-diagonal elements are of the form

$$\sum_{i,j} q_i q_j / r_{ij}$$

where the q 's are monopole charge distributions obtained from some approximate wave function, in this case that of Nagakura (12) as modified by Woody (13). The rows in \mathbf{u} are given by

$$\sum_i q_i \mathbf{P}_i$$

where \mathbf{P}_i is the position vector locating the i th monopole. The rows in \mathbf{m} for the $\pi-\pi^*$ transitions are $i\pi\omega\mathbf{r} \times \mathbf{u}$ where ω is the transition frequency in cm^{-1} , and \mathbf{r} is the center of the $\pi-\pi^*$ transition. Each row in \mathbf{m} for the $n-\pi^*$ transition represents the large intrinsic magnetic moment and is given by $0.468 i$ Bohr magnetons along the OC' bond (13). Diagonalization of \mathbf{H} gives \mathbf{T} and the products $(T\mu)_k(T\mu)_k$ and $\text{Im}(T\mu)_k(Tm)_k$ give the αN absorption and rotational strengths, respectively. Specification of a 10-nm bandwidth allows one to obtain gaussian absorption and circular dichroism spectra. The Kronig-Kramers transform to rotatory dispersion (14) and the extraction of the b_0 parameter have been described (15). Experimentally, highly purified gramicidin S displays a b_0 value of $-720^\circ \pm 90^\circ$ (16).

According to the theoretical formalism outlined above, only one of the three geometries leads to a significantly large negative b_0 (Table 1). This geometry is the one first proposed in detail as a model for gramicidin S by Stern *et al.* (7). The large negative b_0 for model I is the result of large negative rotational strength in the 225-nm region and also reflects the geometry-dependent exciton interactions among the $\pi-\pi^*$ transitions.

Model II, which consists of two short twists of alpha helix joined through the proline and phenylalanine residues, yields a very small and positive b_0 reflecting the effect on the amide optical activity of the proline and phenylalanine residues. Parameters derived from polymer spectra, and especially the b_0 scale of helix content should probably not be used to describe small peptides, particularly cyclic ones.

Rigorous confidence limits cannot be given for the calculated b_0 values, but it is undoubtedly significant that the calculated b_0 of -356° for a linear alpha helical decamer is close to the value of approximately -300° reported for γ -methyl-L-glutamate decamers in dimethylformamide (17).

Not all of the most favorable local energy minimum conformations of gramicidin S have been determined. Nor have biopolymer optical spectral calculations yet reached that stage which would allow a complete screening of the low-energy conformations. However, since the number of local energy minimums for complex peptides and proteins rises rapidly with increasing chain length, even partial screening will be useful.

E. S. PYSH

*Metcalf Research Laboratory,
Brown University,
Providence, Rhode Island 02912*

References and Notes

1. L. C. Craig, *Proc. Nat. Acad. Sci. U.S.A.* **61**, 152 (1968).
2. D. C. Hodgkin and B. M. Oughton, *Biochem. J.* **65**, 752 (1957).
3. R. Schwyzler, in *Amino Acids and Peptides with Antimetabolic Activity*, G. E. W. Wolstenholme and C. M. O'Connor, Eds. (Churchill, London, 1958), p. 171.
4. D. Balasubramanian, *J. Amer. Chem. Soc.* **89**, 5445 (1967); F. Quadrifoglio and D. W. Urry, *Biochem. Biophys. Res. Commun.* **29**, 785 (1967).
5. S. L. Laiken, M. P. Printz, L. C. Craig, *Biochemistry* **8**, 519 (1969).
6. R. Schwyzler and U. Ludescher, *ibid.* **7**, 2519 (1968).
7. A. Stern, W. A. Gibbons, L. C. Craig, *Proc. Nat. Acad. Sci. U.S.A.* **61**, 734 (1968).
8. H. A. Scheraga, S. J. Leach, R. A. Scott, G. Nemethy, *Discuss. Faraday Soc.* **40**, 268 (1965); A. M. Liquori, P. De Santis, A. L. Kovacs, L. Mazzarella, *Nature* **211**, 1039 (1966); G. Vanderkooi, S. J. Leach, G. Nemethy, R. A. Scott, H. A. Scheraga, *Biochemistry* **5**, 2991 (1966).

9. R. A. Scott, G. Vanderkooi, R. W. Tuttle, P. M. Shames, H. A. Scheraga, *Proc. Nat. Acad. Sci. U.S.* **58**, 2204 (1967).
10. F. A. Momany, G. Vanderkooi, R. W. Tuttle, H. A. Scheraga, *Biochemistry* **8**, 744 (1969).
11. E. S. Pysh, *J. Chem. Phys.*, in press.
12. S. Nagakura, *Bull. Chem. Soc. Jap.* **25**, 164 (1952).
13. R. W. Woody, *J. Chem. Phys.* **49**, 4797 (1968).
14. A. Moscovitz, *Advan. Chem. Phys.* **4**, 67 (1962).
15. P. J. Urnes and P. Doty, *Advan. Protein Chem.* **16**, 401 (1961).
16. M. A. Ruttenberg, T. P. King, L. C. Craig, *J. Amer. Chem. Soc.* **87**, 4196 (1965); *Biochemistry* **5**, 2857 (1966). The b_0 for hydrogenated gramicidin S would provide a better comparison since the contribution to optical activity of aromatic side chains was not taken into account in this calculation, but the value has not been reported. However the circular dichroism data of S. Laiken, M. Printz, and L. C. Craig [*J. Biol. Chem.* **244**, 4454 (1969)] on highly purified hydrogenated gramicidin S show qualitatively the same features as untreated gramicidin S and indicate that the b_0 value would be large and negative.
17. M. Goodman, E. E. Schmitt, I. Listowsky, F. Boardman, I. G. Rosen, M. A. Stake, in *Polyamino Acids, Polypeptides and Proteins*, M. A. Stahmann, Ed. (Univ. of Wisconsin Press, Madison, 1962), p. 195.
22. Supported in part by PHS grant GM-14689 and NSF grant GP-4825.

20 October 1969

drite, it seemed possible that the developmental patterning of such synaptic connections may underlie, or be related to, later behavioral flexibility.

Electron microscope studies have demonstrated that the dendrite spine is a distinctive feature of the postsynaptic apparatus in cerebral cortex, cerebellum, brain stem, and spinal cord (3). These lateral extensions of the dendrites were first described by Cajal (4) and, although initially considered an artifact, are now recognized as representing "specific postsynaptic receptive structures on the dendrites" (5). The cortical dendrites of the neonatal kitten do not have spines, and the few qualitative studies performed (5) indicate that they appear slowly during development in association with increasingly complex behavioral and neurophysiological changes. In the rat, spines are also absent at birth and only obtain adult values shortly after weaning (6). The identity of these structures with functional units of the central nervous system (the synapse) and their gradual appearance during development suggest that their ontogeny may in some manner be related to later behavior.

Decreased visual stimulation (7) or interruption of the visual pathway (8) during periods of spine development results in a decreased number of spines in the adult animal, and handling during the early postnatal period increases the rate of formation of new cells in the cerebellum (9). Other investigators (10) experimenting with sensory-enriched or sensory-deprived environments have concentrated upon manipulating the environment after weaning. The rat brain at this time is essentially mature as judged by biochemical, neurophysiological, and morphological criteria (11), and its period of plasticity is largely over. It was suggested earlier (12) that sensory input during maturation of the dendrite spines may accelerate their development and that this differential acceleration of specific neuron processes with their interconnections may represent the neuroanatomical basis for the effects of early experience on subsequent behavior. We designed an experiment to test this hypothesis by initiating diverse sensory stimulation prior to weaning, during the period of central nervous system (CNS) maturation.

Separate litters of Sprague-Dawley rats bred in this laboratory were used. From the day of birth until they were killed at 8 days of age, random litters were either left untouched or were re-

Early Experience Effects upon Cortical Dendrites: A Proposed Model for Development

Abstract. We studied the effects of environmental stimulation on the development of rat cortical pyramidal cell synaptic loci (dendritic spines) and the number of such cells staining by the rapid Golgi technique. Stimulation three to five times a day from the day of birth increased the number of spines per micrometer in 8-day-old animals and increased the number of neurons staining at 8 to 16 days of age. This effect of afferent input upon development of the dendritic spine may represent the neuroanatomical basis for the influence of early experience on subsequent behavior. The number of neurons staining by the rapid Golgi technique appears to be related to those that are functionally involved at the time of tissue preparation.

It is generally accepted that environmental influences during certain periods of early postnatal life have an effect upon later development and behavior (1). The mechanisms whereby early experience induces such long-lasting, and perhaps permanent, effects upon the behavior of the organism are unclear.

Hebb has suggested (2) that the richness of neuronal interconnections represents the neuroanatomical substrate of behavior. As functional contact between two neurons is established when the presynaptic elements of one axon make contiguous contact with the postsynaptic elements of an adjacent den-

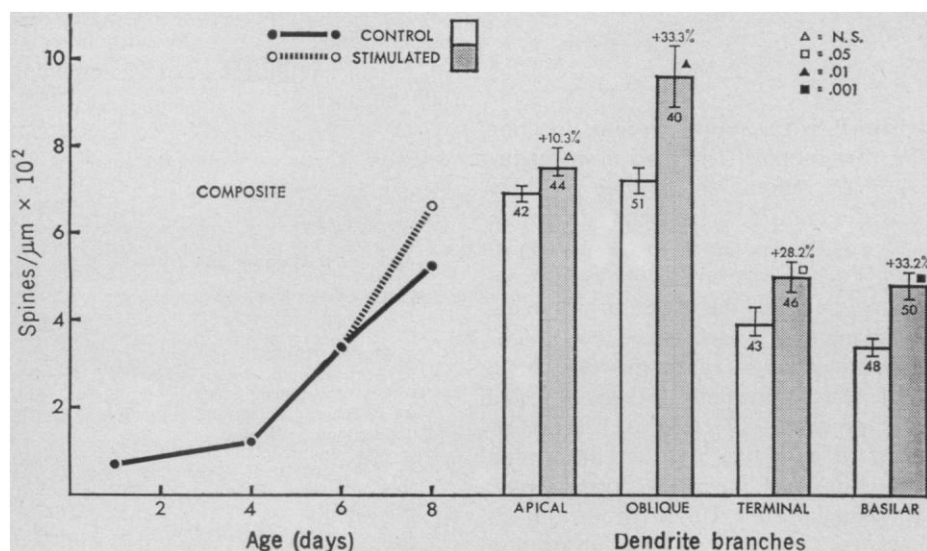


Fig. 1. Effects of environmental stimulation upon spine development on four different dendritic branches of the cortical pyramidal cells. Animals were treated as described. The numbers in the bar graph are the numbers of neurons from which the indicated values for dendritic spines on the various branches were determined. Animals are 8 days old. The composite graph illustrates the average number of spines per micrometer of all dendrite branches covered in the four dendritic locations specified. All values shown for dendrite branches include S.E.'s and are derived from five control and five stimulated animals.